Generation of virtual potentials by controlled feedback in electric circuit systems

Hsin Chang, Kuan-Hsun Chiang, Yonggun Jun, Pik-Yin Lai, and Yung-Fu Chen[*]
Department of Physics and Center for Complex Systems, National Central University, Zhongli 32001, Taiwan

(Received 27 July 2020; accepted 30 March 2021; published 27 April 2021)

Electric circuits influenced by thermal noise are analogous to confined Brownian particles and can be an alternative and convenient scheme for studying stochastic thermodynamics. Here we experimentally demonstrate an effective technique of generating tunable potentials for Brownian dynamics in an electric circuit, realized by external controlled feedback. We present two illustrative examples of one-dimensional virtual potentials: static harmonic potential and time-varying double-well potential. The thermal noises of both cases undergo equivalent Brownian dynamics as if they were in the authentic potentials as long as the feedback is fast enough to respond to the designed potentials. The results show that the electric circuit provides a simple, effective, and programmable scheme to study the feedback-controlled virtual potential.

DOI: 10.1103/PhysRevE.103.042138

I. INTRODUCTION

For the last several decades, there have been technological advances to trap and manipulate nanosized molecules, which have brought a new era for the experimental study in stochastic and information thermodynamics. One of the most popular tools is the optical tweezers, which were employed in many frontier experiments, such as demonstrating Kramers transition rate [1], stochastic resonance [2], Landauer's erasure principle [3], and autonomous and cyclic heat engines [4–6]. Despite the great success with the optical tweezers, further investigation to solve complicated problems such as the dynamics in nonharmonic potentials requires more advanced tools to manipulate the shape of the potentials.

One technique to generate an arbitrary potential is the feedback trap, which applies a feedback force based on a molecule's measured position [7,8]. Cohen first reported a feedback technique to confine a Brownian particle in arbitrary virtual potentials using the image processing technique and the electrophoretic force [9]. Jun and Bechhoefer carefully examined the effects of delay and discrete updates in the feedback process and confirmed the eligibility of using feedback virtual potentials for stochastic thermodynamics studies [10]. The technique was applied to the verification of Landauer's principle with high precision [11]. Recently, replacing the electrophoretic force by the optical force and the CCD camera by the photosensitive device further improves the limitation of the feedback trap caused by the long delay; such a scheme is named the optical feedback trap [12,13]. The performance of the optical feedback trap is highly desirable for nonequilibrium stochastic thermodynamics investigations and has been applied to the problems of shortcut processes connecting equilibrium states [14,15], the colloidal heat engine [16], and the Mpemba effect [17]. Nevertheless, working with the optical feedback trap requires heavy experimental overheads, such as maintaining the stability of the lasers, good optical alignment precision, etc.

It is known that analog simulators can help to investigate behaviors of stochastic and/or chaotic systems ruled by stochastic, nonlinear differential equations [18]. Numerically solving stochastic, nonlinear differential questions typically involves integration over time, which might accumulate errors out of long time integrations for studying low-frequency characteristics. Also as the degrees of freedom of a studied system increases, the need of numerical computation resources rises dramatically. Analog simulations surpass these issues for they are carried out via time evolution of physical electric circuits. Successful examples include stochastic resonance [19] and coupled nonlinear oscillators [20].

Inspired by the pioneering idea of analog simulations, we look for a convenient experimental system via an electric circuit for studies requiring virtual potential generation. The dynamics of accumulated charges on the capacitor of a resistor-capacitor (*RC*) circuit is entirely analogous to the dynamics of an overdamped Brownian particle trapped in a harmonic potential well [21], encouraging us to create feedback virtual potentials in electric circuits. Several advantages of the usage of electric circuit systems are remarkable. Electric systems grant a variety of choices for a random state variable, ranging from the discrete charge state in the single-electron device [22] to a continuous charge variable in the *RC* circuit [21]. In addition, electrostatic energy stored in capacitors, which is the key energy scale of electric systems, is easy to set as compared to thermal energy k_BT, where k_B is the Boltzmann constant, and T is the temperature of the environment so that electric systems could dwell in a regime where stochastic processes are apparent. Moreover, typically, experimental setups of electric systems are relatively simple [23–26] and are often more straightforward to couple together [27] and to scale up.

Here, we report a simple and effective electric-circuit scheme for creating virtual potentials, experimentally establish this idea with ultrafast feedback controls offered by a

[*]yfuchen@cc.ncu.edu.tw

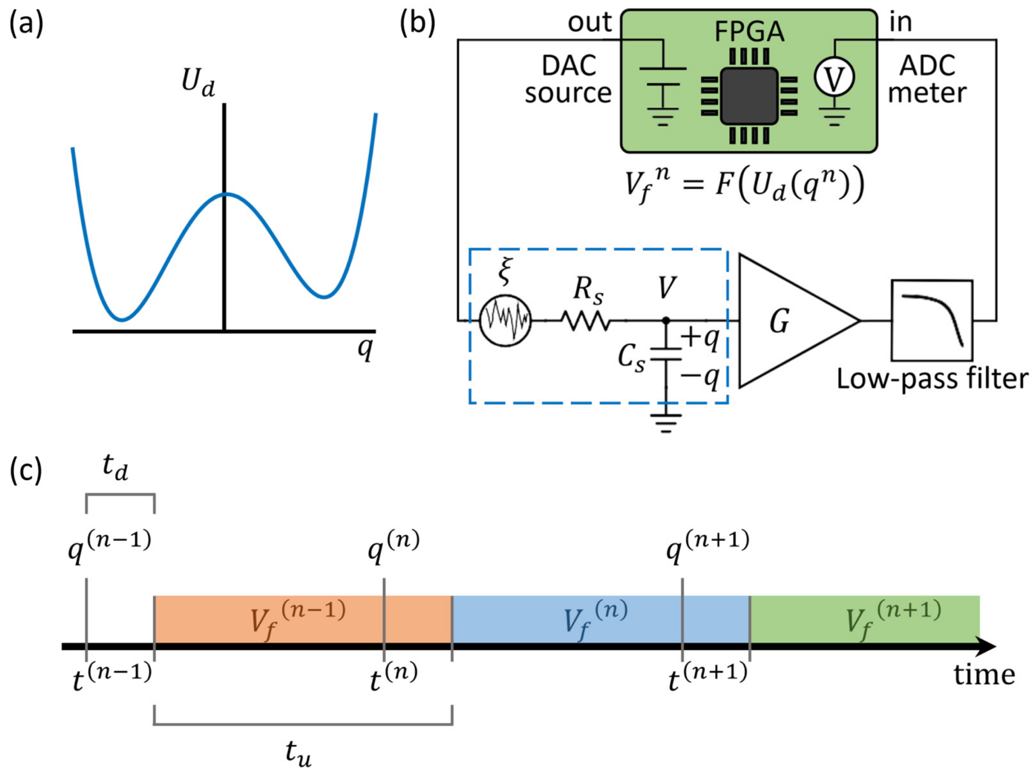

FIG. 1. Feedback-controlled virtual potential. (a) Schematic of an analogous particle confined in a designed virtual potential U_d. (b) Schematic diagram of the experiment setup to realize feedback-controlled virtual potential. The system mainly consists of an *RC* circuit circled by a dashed line, and a FPGA board for sampling the position q, calculating the required feedback, and producing the feedback voltage V_f. ξ represents the thermal noise from the resistor. A voltage preamplifier is used to magnify the voltage signal $V(t)$ with signal level of the order of microvolts before sampling by FPGA. A low-pass filter is introduced after the preamplifier to prevent the aliasing effect caused by the high-frequency white noise from the preamplifier. (c) The timing diagram of the feedback system. The FPGA samples $q^{(n)}$ at $t^{(n)}$ and begins to apply the feedback voltage $V_f^{(n)}$ after a delay time t_d due to the required signal processing time. $q^{(n)}$ is sampled every time interval t_u, and each $V_f^{(n)}$ lasts for the same time interval t_u.

field-programmable gate array (FPGA) device, and characterize the effects of discreteness and delay of feedback in a virtual harmonic potential. With the justification of the validity of dynamics in the discrete system, we investigate the dynamics of stochastic resonance in a time-varying virtual double-well potential. Our studies confirm that the system behaves as if it is in the authentic potentials, and validate that our feedback trap is well suited for the study on nonequilibrium thermodynamics and information thermodynamics under the time-dependent protocol. Moreover, the methodology can be generalized to multidimensional systems, which could even outperform numerical studies regarding time efficiency.

For an *RC* circuit analogous to an overdamped Brownian particle trapped in a designed one-dimensional (1D) virtual potential $U_d(q)$, as illustrated in Fig. 1(a), the motion obeys the Langevin equation

$$-R_s\dot{q} - \frac{d}{dq}U_d + \xi = 0, \tag{1}$$

where q is the accumulated charge on the capacitor C_s and stands for the dynamical coordinate of the system, $-R_s\dot{q}$ represents the damping due to charge flowing through the resistor R_s, $-\frac{d}{dq}U_d$ represents the conservative force originated by the designed virtual potential, and ξ is Johnson-Nyquist noise from the resistor and represents the random thermal force [28,29]. The thermal noise has zero mean $\langle\xi(t)\rangle = 0$, and has no time correlation $\langle\xi(t)\xi(t')\rangle = 2k_BTR_s\delta(t-t')$, where $\delta(t-t')$ is the Dirac delta function. Figure 1(b) shows the schematic of the system to realize the virtual potential generation. An FPGA device is used to record the coordinate $q(t) = C_sV(t)$ at the moment t via sampling the voltage $V(t)$, and to immediately output a corresponding voltage $V_f[q(t)]$. In accordance with Kirchhoff's law, the equation of motion of the circuit is

$$-R_s\dot{q} + V_f - q/C_s + \xi = 0. \tag{2}$$

As long as $V_f = -dU_d/dq + q/C_s$ is applied and updated immediately and constantly according to $q(t)$, the dynamic of the system will resemble the dynamic governed by Eq. (1), therefore creating the designed virtual potential $U_d(q)$. However, in reality, the feedback voltage provided by the digital instrument is discrete in time and has delay.

As Fig. 1(b) depicts, the experimental setup to realize the feedback-controlled virtual potential consists of a resistor $R_s = 9.13$ MΩ in parallel with a capacitor $C_s = 42.4$ pF, holding a time constant $\tau_s = R_sC_s = 387$ μs. Before sampling, the voltage $V(t)$ across the capacitor C_s is magnified by a voltage preamplifier (SR560) with a gain of 1000 and an

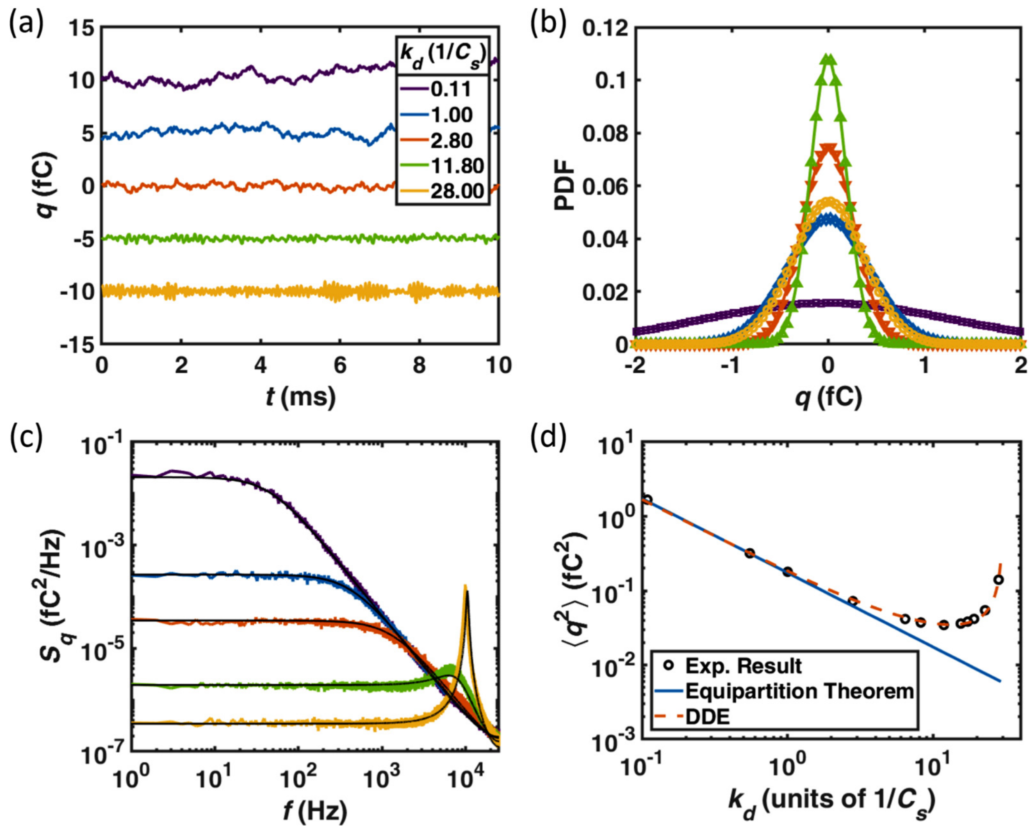

FIG. 2. Virtual harmonic potential. (a) Trajectories of analogous particle with various designed stiffness k_d. (b) Probability distribution $P(q)$ and (c) power spectral density $S_q(f)$ from the trajectories in (a). The black lines in (c) are given from Eq. (A9). (d) Plot of the variance $\langle q^2\rangle$ as a function of k_d. The symbols are the data. The blue solid line indicates $\langle q^2\rangle = k_BT/k_d$, the prediction of equipartition theorem for real harmonic potential confinement. The red dashed line is the fitting curve Eq. (A4) from the result of the delay differential equation.

added noise of 1.6×10^{-17} V^2/Hz above 1 kHz. The white noise added by the preamplifier is removed by a low-pass *RC* filter with a cutoff frequency of 50 kHz to avoid aliasing effect. The FPGA board (NI sbRIO-9637) is used to sample $V(t)$ via an analog-to-digital converter (ADC) with sampling time $t_s = 20$ μs, and to calculate the corresponding feedback voltage V_f, and to apply V_f via a digital-to-analog converter (DAC) with update time $t_u = t_s = 20$ μs. Note that $t_u \ll \tau_s$ indicates that the feedback control updates constantly while the system does not respond too much to the feedback voltage and the thermal noise and is a key criterion for the feedback virtual to function properly. The system is placed at room temperature $T = 296$ K.

II. VIRTUAL HARMONIC POTENTIAL

The first demonstration of virtual potentials for the analogous particle is a 1D static harmonic potential $U_h = (k_d q^2)/2$, where k_d is the designed stiffness. The corresponding feedback voltage $V_{f,h}[q = q(t - t_d), t] = (-k_d + 1/C_s)q$. Figures 2(a)–2(c) depict the trajectory $q(t)$, the probability density function (PDF) $P(q)$, and the power spectral density $S_q(f)$, respectively, for various k_d. At small k_d, such as $k_d = 0.11/C_s$, $1/C_s$, and $2.80/C_s$, the fluctuation of the system is suppressed as k_d increases. $P(q)$ has a Gaussian distribution $P(q) \propto \exp{(-q^2/2\sigma^2)}$ with the variance $\sigma^2 = \langle q^2\rangle = k_BT/k_d$, and $S_q(f)$ behaves like a Lorentzian function $S_q(f) = S_q(0)/[1 + (f/f_c)^2]$ with a plateau at the level $S_q(0) = 4k_BTR_s/k_d^2$ and the cutoff frequency at $f_c = k_d/2\pi R_s$. Figure 2(d) shows $\langle q^2\rangle$ as a function of k_d, where the symbol corresponds to the data and the blue solid line indicates the prediction from the equipartition theorem $\langle q^2\rangle = k_BT/k_d$. The behaviors are compatible with those of a particle sitting in a real harmonic potential with the designed stiffness and can be accurately explained by the fluctuation-dissipation theorem (FDT) [21]. Note that the case of $k_d = 1/C_s = 23.6$ V/nC requires no feedback, and the system is in an unengineered harmonic potential $U_h = q^2/2C_s$. The root mean square of fluctuation is $q_{\rm rms} = \sqrt{k_BTC_s} = 0.416$ fC. Also for the case of $k_d = 0$, the analogous particle experiences no trapping force and behaves like a free diffusion motion.

As k_d becomes large, the behaviors of the electric circuit in the virtual harmonic potential deviate from the expectation of FDT. The discrepancy is due to the imperfect feedback in the system. The feedback cannot respond instantly enough to mimic the target harmonic system with a large k_d [10]. Figure 1(c) illustrates the time sequence of feedback in the system. The ADC of the FPGA board samples the voltage signal $V(t)$ every time interval t_u and converts it to the analogous particle position. $q^{(n)} = q(t^{(n)}) = C_sV(t^{(n)})$ represents the position sampled at $t^{(n)}$. The feedback reacts by applying the feedback voltage $V_f^{(n)} = V_f(q^{(n)})$ via the DAC of the

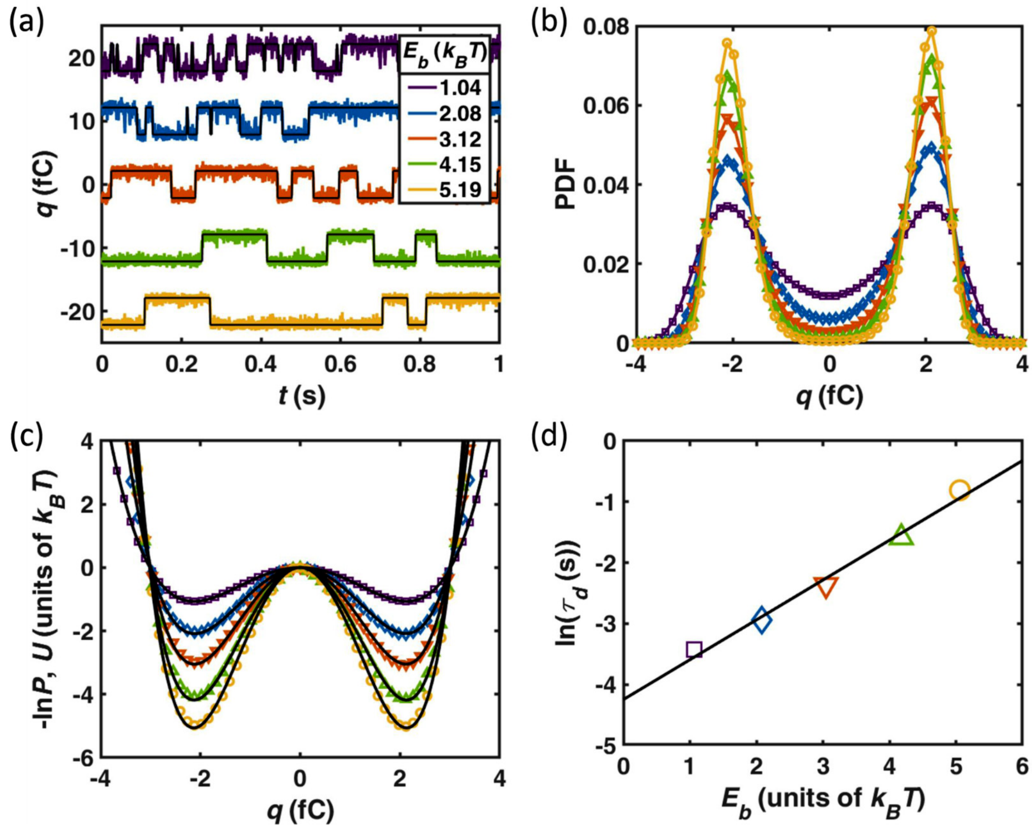

FIG. 3. Virtual double-well potential. (a) Trajectories of the analogous particle in double-well potential with fixed $q_m = 2.12$ fC and various E_b. (b) Probability distribution $P(q)$ of the trajectories in (a). (c) Derived potential $U_d(q) = -k_BT \ln P(q)$ from the distribution in (b). The symbols represent the derived potentials, and black lines are the fit to the double-well potential. The designed values and fitting parameters of q_m and E_b are listed in Table I. (d) Dwelling time τ_D with various E_b in a log-log plot. The black line denotes the Kramers relation $\tau_D \propto \exp(E_b/k_BT)$.

FPGA after the delay time t_d, and lasting for a time t_u. At large k_d, the virtual force is large for the system away from potential minimum. Even within small t_d, $q(t^{(n)} + t_d)$ can be quite different from $q^{(n)}$. Consequently, the required feedback voltage $V_f[q(t^{(n)} + t_d)]$ for the moment $t^{(n)} + t_d$ could be very different from the applied feedback voltage $V_f^{(n)}$. The finite t_u has a similar effect. The required feedback voltage between $t^{(n)} + t_d$ and $t^{(n)} + t_d + t_u$ is different from $V_f^{(n)}$. The finite t_u possibly causes the particle to overreact, resulting in a broader distribution in $P(q)$.

To fully understand the influence of the discrete update and finite delay time quantitatively, we consider a discrete sampling version of the equation of motion to describe the dynamics of the analogous particle in the Appendix. The red dashed curve in Fig. 2(d) shows the fit of the data $\langle q^2 \rangle$ as a function of k_d to Eq. (A4) in the Appendix. The consideration of discrete feedback and delay captures the behaviors of the system reasonably well. The delay time of the feedback, $t_d = 13.3\ \mu$s, is determined by the fitting. The behaviors of $S_q(f)$ are also predicted by Eq. (A9). At small k_d ($k_d \ll 8.49/C_s$), Eq. (A9) reduces to the Lorentzian function, corresponding to $S_q(f)$ of a Brownian system sitting in a real harmonic potential with the designed k_d. At very large k_d ($k_d > 8.49/C_s$), a resonance is predicted as described in the Appendix. The black curves in Fig. 2(c) are the theoretical predictions given by Eq. (A9), which precisely match with the experimental data. Note that no fitting procedure is performed here. The theory successfully explains the experimental observation, demonstrating the validity of our theoretical understanding of the controlled-feedback virtual potentials.

III. VIRTUAL DOUBLE WELL

Next, the analogous particle is engineered to sit in a virtual double-well potential. The form of the double-well potential is $U_{\rm dw} = E_b[(\frac{q}{q_m})^4 - 2(\frac{q}{q_m})^2]$, where E_b is the barrier height between the two wells, and q_m is the distance of the local minima from the barrier peak. Figure 3(a) shows the experimental trajectories of the system in a virtual double-well potential with fixed $q_m = 2.12$ fC and different designed E_b (in a unit of k_BT). The system sits around one of the local minima at $\pm q_m$, jumping back and forth stochastically between two wells. The black lines in Fig. 3(a) are the location of the well and resemble random telegraph signals, typical for a particle trapped in a potential with two local minima and agitated by random noise for hopping transitions. As E_b increases, the jumps occur less frequently, corresponding to an increase of the dwell time τ_D in a well. The probability distributions $P(q)$ of various trajectories are depicted in Fig. 3(b). The distributions display two peaks. Figure 3(c) shows $-\ln P(q)$ (symbols) and their fit

TABLE I. Comparison of the designed values and the fitting results for the parameters of virtual double-well potential in Fig. 3.

	E_b (k_BT)		q_m (fC)	
	Designed	Fitting	Designed	Fitting
$E1$	1.04	1.07	2.12	2.13
$E2$	2.08	2.08	2.12	2.12
$E3$	3.12	3.05	2.12	2.12
$E4$	4.15	4.18	2.12	2.13
$E5$	5.19	5.06	2.12	2.13

to $U_{dw}(q)/k_BT$ with two fitting parameters E_b and q_m (curves). Table I compares the fitting values with the designed ones, and the agreement demonstrates the precision of the generation of virtual double-well potential. The average dwell time $\langle\tau_D\rangle$ as a function of E_b is depicted in Fig. 3(d). The data is adequately described by the Kramers relation $\langle\tau_D\rangle \propto \exp(E_b/k_BT)$, indicating that the transitions between two wells are governed by thermal excitation.

IV. TILTING DOUBLE WELL

We also demonstrate the generation of a time-independent tilting double well $U_{\rm tdw} = E_b[(\frac{q}{q_m})^4 - 2(\frac{q}{q_m})^2 + 4A_t(\frac{q}{q_m})]$, where A_t characterizes the amplitude of the tilt. $|A_{t,\rm cr}| = 2/(3\sqrt{3})$ is the critical value for disappearance of the minor well. The symbols in Figs. 4(a) and 4(b) show the PDF and corresponding $-\ln P(q)$ for the designed $E_b = 3.12k_BT$ and $A_t = \pm 0.06$. The black lines in Fig. 4(b) simply plot the designed $U_{\rm tdw}$.

Finally, we present a study of the time-varying virtual potential to demonstrate the competence of using virtual potentials for investigating nonequilibrium stochastic thermodynamics. It is known that stochastic resonance [30,31] occurs in the periodic tilting double-well system with an adequate noise level [32]. We add a time-varying periodic tilt term to the tilting double-well potential, $U_{\rm tdw}(t) = E_b[(\frac{q}{q_m})^4 - 2(\frac{q}{q_m})^2 + 4A_t\cos(2\pi f_t t)(\frac{q}{q_m})]$, where f_t represents the frequency of the time-dependent tilt. This extra time-varying tilt term makes the double-well global minimum switch between the left and the right well alternately with the frequency f_t. For $|A_t| > |A_{t,\rm cr}|$, the minor well will disappear when the tilting is maximal within a period.

Figure 4(c) shows the trajectories of the system for $A_t = 0.2$, $f_t = 10$ Hz, and various barrier height E_b. At large E_b, such as $E_b = 3.12$, 4.15, and $5.19k_BT$, the analogous particle jumps between two wells occasionally, which is typical for fixed double-well potentials. As E_b decreases and the transition rate of the corresponding E_b is close to twice

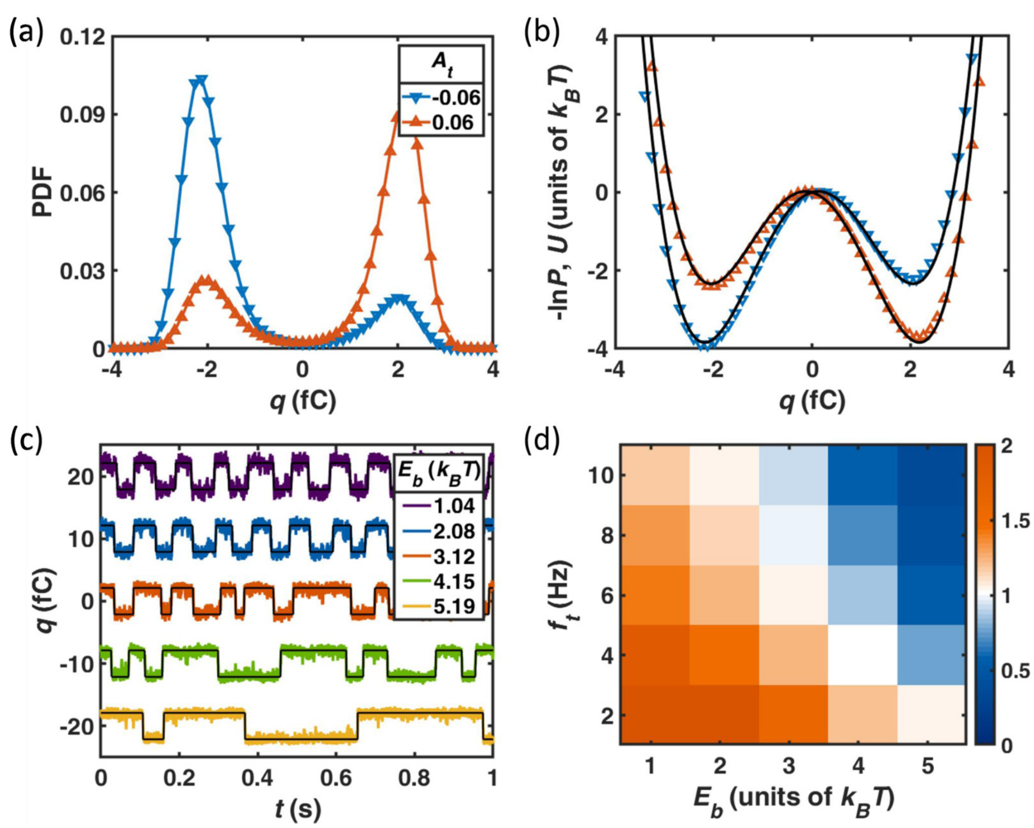

FIG. 4. Demonstration of tilting double well and stochastic resonance. (a) PDF $P(q)$ of time-independent tilting double well for $E_b = 3.12k_BT$ and $A_t = -0.06$ (blue inverted triangle) and $+0.06$ (red triangle), respectively. (b) Effective potential $U_d(q)$ from the distributions in (a). The symbols denote the effective potential, and the black lines plot the designed static tilting double-well potential. (c) Trajectory response of the analogous particle in a periodic tilt double-well potential for $A_t = 0.2$, $f_t = 10$ Hz, and various E_b. (d) The map of $1/2f_t\langle\tau_D\rangle$ with fixed $A_t = 0.2$ for various E_b and f_t. The white color-mapping denotes $f_t = 1/2\langle\tau_D\rangle$, which is the region that stochastic resonance occurs.

the modulation frequency, namely, $1/\langle\tau_D\rangle \approx 2f_t$, the system begins to travel back and forth between the two wells periodically with a frequency that coincides with the tilting frequency of the virtual double-well potential, as shown for the cases of $E_b = 1.04$ and $2.08k_BT$. The behavior of the system synchronizes with the control of virtual double-well potential when the thermal noise level and the size of the tilt are appropriate, i.e., stochastic resonance occurs. Figure 4(d) shows the map of transition rates to the modulation frequency ratio $1/2f_t\langle\tau_D\rangle$ as a function of E_b for $f_t = 2$, 4, 6, 8, and 10 Hz with fixed $A_t = 0.2$. The region, where stochastic resonance occurs, is shown in white color-mapping. The light-red color signifies the cases of $1/2\langle\tau_D\rangle$ larger than the modulation frequency f_t, and the dark-blue color represents the opposite case. One can see that at $f_t = 2$ Hz, stochastic resonance occurs at $E_b = 5.19k_BT$. As f_t increases, the resonance locates at decreasing E_b. This implies that the proper transition rate induced by thermal noise is important for observing the occurrence of stochastic resonance.

V. CONCLUSION

In conclusion, we have successfully demonstrated several feedback-controlled virtual potentials in the *RC* electric circuit system and analyze the dynamics of the analogous particle confined in the potentials. We also study the limitation of the feedback due to the delay and the discrete nature of the update in the linear harmonic potential. The demonstration of the double-well potential generalizes the applications of virtual potential to nonlinear cases. The time-varying protocol of virtual double-well potential shows the dynamical behaviors are consistent with the phenomenon of stochastic resonance, and illustrates the applicability of this simple, effective, and programmable system to studies in stochastic thermodynamics, nonequilibrium steady-state dynamics, heat engines, and information topics. We stress that the virtual potential system we demonstrated here is only 1D. The methodology can, in principle, be generalized to systems with multi degrees of freedom. The generalization could be relevant to a broad range of applications. For instance, the features of the Brownian gyrator [26,33] can be observed by coupling two *RC* circuits with a feedback function instead of a coupling capacitor. The technique opens the possibility of studying nonequilibrium steady-state dynamics in the sophisticated, nonlinear high-dimensional virtual potentials created by feedback control.

ACKNOWLEDGMENTS

We acknowledge support from the Ministry of Science and Technology in Taiwan under Grants No. 109-2112-M-008-006 (Y.J.) and No. 107-2112-M-008-013-MY3 (P-Y.L.), and the NCTS of Taiwan (P-Y.L.).

APPENDIX: DISCRETE ANALYSIS OF POWER SPECTRAL DENSITY

Here we perform discrete analysis to derive the power spectral density of the feedback control system for the generation of a virtual harmonic potential. Consider the feedback system with a finite updating time t_u and sampling time t_s, and take $t_u = t_s$. By the Wiener-Khinchin theorem, the power spectral density of a discrete-time random process is given by the discrete Fourier transform of its autocorrelation function, i.e.,

$$S_q(f) = 2t_u \sum_{k=-\infty}^{\infty} R_k \exp(-i2\pi f t_u k), \tag{A1}$$

where $R_k = \langle q^{(n)} q^{(n-k)}\rangle$ denotes the discrete autocorrelation function of $q(t)$. As long as the analytical expression of R_k is available, $S_q(f)$ can be determined via Eq. (A1).

Incorporating Eq. (2) and feedback voltage $V_{f,h}$ with the time sequence of the feedback in Fig. 1(c), the evolution of q sampled at discrete times can be written as

$$q^{(n+1)} = q^{(n)} + (1 - C_s k_d)\left(\frac{t_d}{\tau_s} q^{(n-1)} + \frac{t_u - t_d}{\tau_s} q^{(n)}\right) - \frac{t_u}{\tau_s} q^{(n)} + \frac{1}{R_s}\xi^{(n)}, \tag{A2}$$

where $\xi^{(n)} \equiv \int_{nt_u}^{(n+1)t_u} \xi(t)dt$ is the impulse due to the random noise in the time interval $[nt_u, (n+1)t_u]$. $\xi^{(n)}$ holds statistical properties of $\langle\xi^{(n)}\rangle = 0$ and $\langle\xi^{(n)}\xi^{(m)}\rangle = 2k_BTR_st_u\delta_{nm}$. For convenience, we define $\beta_d \equiv t_d/\tau_s$ and $\beta_u \equiv t_u/\tau_s$, and Eq. (A2) is simplified to

$$q^{(n+1)} = a_1 q^{(n)} - a_2 q^{(n-1)} + \frac{1}{R_s}\xi^{(n)}, \tag{A3}$$

where $a_1 = 1 - (C_s k_d - 1)(\beta_u - \beta_d) - \beta_u$ and $a_2 = (C_s k_d - 1)\beta_d$. The variance of q can be given by $R_0 = \langle q^2\rangle = (a_1^2 + a_2^2)\langle q^2\rangle - 2a_1a_2\langle q^{(n)}q^{(n-1)}\rangle + \frac{\langle\xi^{(n)2}\rangle}{R_s^2}$ and the correlation term is $R_1 = \langle q^{(n)}q^{(n-1)}\rangle = \frac{a_1}{1+a_2}\langle q^2\rangle$. Thus, we obtain $R_0 = \frac{\langle\xi^{(n)2}\rangle(1+a_2)/R_s^2}{(1-a_2)[a_2-(a_1-1)][a_2+(a_1+1)]}$, or

$$\langle q^2\rangle = \frac{2k_BT[1 + (C_s k_d - 1)\beta_d]}{k_d[1 - (C_s k_d - 1)\beta_d][2(1 - \beta_d) - (\beta_u - 2\beta_d)C_s k_d]}. \tag{A4}$$

When $k_d \ll 1/C_s\beta_u, 1/C_s\beta_d$ and $\beta_u, \beta_d \ll 1$, the feedback is fast enough to react for designed potentials, and Eq. (A4) reduces to the equipartition theorem $\langle q^2\rangle = k_BT/k_d$. As k_d gets large while the response times of the feedback stay fixed, the feedback does not react fast enough for the designed potential, and $\langle q^2\rangle$ becomes larger than the expectation of the equipartition theorem. At very large k_d, the system becomes highly agitated, $\langle q^2\rangle$ increases with k_d, and even some resonant behavior develops. A resonant structure arising around the inverse of the response time t_u and t_d is clearly seen in the power spectral density $S_q(f)$ for very large k_d in Fig. 2. Equation (A4) diverges at $k_d = \frac{1+\beta_d}{\beta_d}\frac{1}{C_s}$, and the motion of the system becomes unstable.

To find out the discrete power spectral density solution, a discrete autocorrelation sequence can be constructed with the definition $r_k \equiv \frac{R_k}{R_0}$,

$$r_0 = 1,$$
$$r_1 = \frac{a_1}{1 + a_2},$$
$$r_k = a_1 r_{k-1} - a_2 r_{k-2}, \quad k > 1. \tag{A5}$$

To derive the expression of the discrete autocorrelation sequence, a geometric sequence is constructed as $r_k - \alpha_+ r_{k-1} = \alpha_-(r_{k-1} - \alpha_+ r_{k-2})$. Compared with Eq. (A3), we obtain $\alpha_\pm = \frac{a_1 \pm \sqrt{\zeta}}{2}$ and a geometric sequence $\{r_k - \alpha_+ r_{k-1}\}$:

$$\begin{aligned} r_k - \alpha_+ r_{k-1} &= \alpha_-^{k-1}(r_1 - \alpha_+ r_0) \\ &= \alpha_-^{k-1}\left[\frac{a_2 - \alpha_+(1+a_2)}{1+a_2}\right], \end{aligned} \tag{A6}$$

where $\zeta = a_1^2 - 4a_2$ can be used for the determination of the damping behavior of r_k. We define $\overline{r_k} = \frac{r_k}{\alpha_-^k}$ and construct a new geometric sequence $\overline{r_k} - \lambda = \frac{\alpha_+}{\alpha_-}(\overline{r_{k-1}} - \lambda)$. Comparing the new sequence with Eq. (A6), we have $\lambda = \frac{1}{2} - \frac{a_1(1-a_2)}{2\sqrt{\zeta}(1+a_2)}$ and $\{\overline{r_k} - \lambda\}$ is also a geometric sequence. Hence $\overline{r_k} - \lambda = (\frac{\alpha_+}{\alpha_-})^k(\overline{r_0} - \lambda) = (\frac{\alpha_+}{\alpha_-})^k(1 - \lambda)$ and we finally obtain the expression of the discrete autocorrelation sequence

$$\begin{aligned} r_k =& \left(\frac{a_1 + \sqrt{\zeta}}{2}\right)^k \left[\frac{1}{2} + \frac{a_1(1-a_2)}{2\sqrt{\zeta}(1+a_2)}\right] \\ &+ \left(\frac{a_1 - \sqrt{\zeta}}{2}\right)^k \left[\frac{1}{2} - \frac{a_1(1-a_2)}{2\sqrt{\zeta}(1+a_2)}\right]. \end{aligned} \tag{A7}$$

Note that there exists a special $k_{d,\mathrm{cr}}$ that makes $\zeta = 0$ and the expression in Eq. (A7) diverges ($k_{d,\mathrm{cr}} = 6.33/C_s$ in our system). The problem can be revised by solving Eq. (A6) with $\alpha_+ = \alpha_-$. As $\zeta < 0$, r_k decays and oscillates near zero, similar to an underdamped oscillation; while $\zeta > 0$, r_k decays to zero exponentially, similar to the overdamped case. We define the special case $k_{d,\mathrm{cr}}$ as critical damped for the fastest damping of r_k, and the autocorrelation expression is

$$r_k = \left(\frac{a_1}{2}\right)^k \left(1 + k\frac{1-a_2}{1+a_2}\right). \tag{A8}$$

Substituting $R_k = R_0 r_k$ into Eq. (A1), we obtain the discrete power spectral density:

$$S_q(f) = \frac{4k_B T t_u^2/R_s}{4a_2\cos^2\theta - 2a_1(1+a_2)\cos\theta + (a_2-1)^2 + a_1^2}, \tag{A9}$$

where $\theta = 2\pi f t_u$. As shown in Fig. 2(c), the theoretical prediction agrees well with the experimental data. To understand the resonant structure for large k_d, we can rewrite the equation as

$$S_q(f) = \frac{4k_B T t_u^2/R_s}{4a_2\left[\cos\theta - \frac{a_1(1+a_2)}{4a_2}\right]^2 + (a_2-1)^2\left(\frac{4a_2 - a_1^2}{4a_2}\right)}. \tag{A10}$$

As $\frac{a_1(1+a_2)}{4a_2} < 1$, $S_q(f)$ has a local maximum at $f_r = \cos^{-1}[\frac{a_1(1+a_2)}{4a_2}]/2\pi t_u$, indicating the resonant behavior of the system.

[1] L. I. McCann, M. Dykman, and B. Golding, Thermally activated transitions in a bistable three-dimensional optical trap, Nature (London) **402**, 785 (1999).

[2] A. Simon and A. Libchaber, Escape and Synchronization of a Brownian Particle, Phys. Rev. Lett. **68**, 3375 (1992).

[3] J. M. R. Parrondo, J. M. Horowitz, and T. Sagawa, Thermodynamics of information, Nat. Phys. **11**, 131 (2015).

[4] I. A. Martínez, É. Roldán, L. Dinis, D. Petrov, J. M. R. Parrondo, and R. A. Rica, Brownian Carnot engine, Nat. Phys. **12**, 67 (2016).

[5] J.-M. Park, H.-M. Chun, and J. D. Noh, Efficiency at maximum power and efficiency fluctuations in a linear Brownian heat-engine model, Phys. Rev. E **94**, 012127 (2016).

[6] A. Argun, J. Soni, L. Dabelow, S. Bo, G. Pesce, R. Eichhorn, and G. Volpe, Experimental realization of a minimal microscopic heat engine, Phys. Rev. E **96**, 052106 (2017).

[7] A. E. Cohen and W. E. Moerner, Method for trapping and manipulating nanoscale objects in solution, Appl. Phys. Lett. **86**, 093109 (2005).

[8] J. Stergar and N. Osterman, Thermophoretic tweezers for single nanoparticle manipulation, Beilstein J. Nanotechnol. **11**, 1126 (2020).

[9] A. E. Cohen, Control of Nanoparticles with Arbitrary Two-Dimensional Force Fields, Phys. Rev. Lett. **94**, 118102 (2005).

[10] Y. Jun and J. Bechhoefer, Virtual potentials for feedback traps, Phys. Rev. E **86**, 061106 (2012).

[11] Y. Jun, M. Gavrilov, and J. Bechhoefer, High-Precision Test of Landauer's Principle in a Feedback Trap, Phys. Rev. Lett. **113**, 190601 (2014).

[12] J. A. C. Albay, G. Paneru, H. K. Pak, and Y. Jun, Optical tweezers as a mathematically driven spatio-temporal potential generator, Opt. Express **26**, 29906 (2018).

[13] A. Kumar and J. Bechhoefer, Nanoscale virtual potentials using optical tweezers, Appl. Phys. Lett. **113**, 183702 (2018).

[14] J. A. C. Albay, S. R. Wulaningrum, C. Kwon, P.-Y. Lai, and Y. Jun, Thermodynamic cost of a shortcuts-to-isothermal transport of a Brownian particle, Phys. Rev. Research **1**, 033122 (2019).

[15] J. A. C. Albay, P.-Y. Lai, and Y. Jun, Realization of finite-rate isothermal compression and expansion using optical feedback trap, Appl. Phys. Lett. **116**, 103706 (2020).

[16] J. A. C. Albay, Z. Zhou, C. Chang, and Y. Jun, Shift a laser beam back and forth to exchange heat and work in thermodynamics, Sci. Rep. **11**, 4394 (2021).

[17] A. Kumar, and J. Bechhoefer, Exponentially faster cooling in a colloidal system, Nature **584**, 64 (2020).

[18] *Noise in Nonlinear Dynamical Systems*, edited by F. Moss and P. V. E. McClintock (Cambridge University Press, Cambridge, UK, 1989), Vol. 3.

[19] T. Zhou and F. Moss, Analog simulations of stochastic resonance, Phys. Rev. A **41**, 4255 (1990).

[20] J. C. Chedjou, H. B. Fotsin, P. Woafo, and S. Domngang, Analog simulation of the dynamics of a van der Pol oscillator coupled to a Duffing oscillator, IEEE Trans. Circ. Syst. I: Fund. Theory Appl. **48**, 748 (2001).

[21] N. Garnier and S. Ciliberto, Nonequilibrium fluctuations in a resistor, Phys. Rev. E **71**, 060101(R) (2005).

[22] V. F. Maisi, O.-P. Saira, Yu. A. Pashkin, J. S. Tsai, D. V. Averin, and J. P. Pekola, Real-Time Observation of Discrete Andreev Tunneling Events, Phys. Rev. Lett. **106**, 217003 (2011).
[23] S. Ciliberto, Experiments in Stochastic Thermodynamics: Short History and Perspectives, Phys. Rev. X **7**, 021051 (2017).
[24] K.-H. Chiang, C.-W. Chou, C.-L. Lee, P.-Y. Lai, and Y.-F. Chen, Fluctuations of entropy production in partially masked electric circuits, Europhys. Lett. **113**, 30001 (2016).
[25] K.-H. Chiang, C.-L. Lee, P.-Y. Lai, and Y.-F. Chen, Entropy production and irreversibility of dissipative trajectories in electric circuits, Phys. Rev. E **95**, 012158 (2017).
[26] K.-H. Chiang, C.-L. Lee, P.-Y. Lai, and Y.-F. Chen, Electrical autonomous Brownian gyrator, Phys. Rev. E **96**, 032123 (2017).
[27] S. Ciliberto, A. Imparato, A. Naert, and M. Tanase, Heat Flux and Entropy Produced by Thermal Fluctuations, Phys. Rev. Lett. **110**, 180601 (2013).
[28] J. B. Johnson, Thermal agitation of electricity in conductors, Phys. Rev. **32**, 97 (1928).
[29] H. Nyquist, Thermal agitation of electric charge in conductors, Phys. Rev. **32**, 110 (1928).
[30] L. Gammaitoni, P. Hänggi, P. Jung, and F. Marchesoni, Stochastic resonance, Rev. Mod. Phys. **70**, 223 (1998).
[31] M. D. McDonnell and D. Abbott, What is stochastic resonance? Definitions, misconceptions, debates, and its relevance to biology, PLoS Comput. Biol. **5**, e1000348 (2009).
[32] R. Benzi, A. Sutera, and A. Vulpiani, The mechanism of stochastic resonance, J. Phys. A: Math. Gen. **14**, L453 (1981).
[33] R. Filliger and P. Reimann, Brownian Gyrator: A Minimal Heat Engine on the Nanoscale, Phys. Rev. Lett. **99**, 230602 (2007).